Thermal Characteristics of Dry Gas Seal in Startup Process Considering Microscale Effects

Qiangguo Deng , Xuejian Sun * , Hengjie Xu , Wenyuan Mao

Posted Date: 9 November 2023

doi: 10.20944/preprints202311.0650.v1

Keywords: dry gas seal; thermal characteristics; slip flow; acceleration mode

Article

Thermal Characteristics of Dry Gas Seal in Startup Process Considering Microscale Effects

Qiangguo Deng [1,2,3], Xuejian Sun [2,*], Hengjie Xu [2] and Wenyuan Mao [2]

[1] Faculty of Environmental Science and Engineering, Kunming University of Science and Technology, Kunming, 650500, China; dengqiangguo@kust.edu.cn
[2] Faculty of Chemical Engineering, Kunming University of Science and Technology, Kunming, 650500, China; 761442586@qq.com(X.S);why_551@kmust.edu.cn(H.X); 183980156@qq.com(W.M)
[3] Faculty of Mechanical and Electrical Engineering, Kunming University of Science and Technology, Kunming, 650500, China
* Correspondence: 761442586@qq.com(X.S)

Abstract: The heat generated during the startup process of dry gas seals, such as the friction heat of the asperities, viscous shear heat, and the expansion heat of the gas film, easily leads to seal failure and endangers the stable operation of turbomachinery. This study combines the statistically modified contact model and the average Reynolds equation by considering the adiabatic index and the microscale effects of dry gas seals to explore the heat generation characteristics of dry gas seals formed in series at multiple times. In particular, the change laws and influencing factors among the components, including the friction heat of asperities and the shear heat and expansion heat of the gas film and total heat, are investigated. A comparative analysis indicates that the slip flow effect increases the total heat during the startup process. The friction heat is much greater than expansion heat and shear heat. Despite constant acceleration, exponential acceleration, or Harrision acceleration, the heat changes are uneven during the startup process. In particular, the heat changes sharply in the early stage and gently in the later stage. The Harrision acceleration mode is the most conducive to sealing stability.

Keywords: dry gas seal; thermal characteristics; slip flow; acceleration mode

1. Introduction

As an advanced noncontact mechanical seal, dry gas seal has been widely applied in rotating equipment, such as large compressors and centrifugal pumps. It has also been developed for high-end turbomachinery, such as aero-engines, the main helium circulator of High temperature steam generator (HTGR), and carbon dioxide reinjection compressors. However, the dry gas seal is still the weak link of turbomachinery, particularly during the startup process of dry gas seals. The friction heat of the asperities on the end face, the viscous shear heat of the gas film, and the gas expansion heat under the seal pressure difference lead to seal failure and endanger the stable operation of turbomachinery. During the startup process of dry gas seal, the rotating speed and sealing clearance vary, and three kinds of heat characteristics change nonlinearly. Determining the heat change on the end face and the balance law of the dry gas seal during the startup process can prevent startup failure and ensure operational stability.

The end face of the dry gas seal is in a contact state in the early startup process, and the heat on the seal face is generated by the asperities and the gas film. When the rotating speed exceeds a certain critical value, the seal face is out of contact, and the heat is generated by the gas film alone. Rahmani et al. [1] used Fluent software to study the performance of a dry gas seal's trapezoidal symmetric grooves by considering heat flow coupling. When the seal face has a small clearance, the contact power loss increases because of the contact effect of the asperities on the sealing ring surface, and the working temperature increases evidently. Xu et al. [2] solved the governing equations of dry gas seal considering gas film pressure, gas temperature, and solid temperature through the finite difference method. The surface deformation of the sealing ring was acquired through the finite element method.

 doi:10.20944/preprints202311.0650.v1

The thermal deformation characteristics of the spiral groove at high temperatures were obtained, and the influencing laws of environmental temperature and temperature difference on the thermal deformation and sealing performance were determined. Salant et al. [3] combined the simultaneous lubrication equation and energy equation, adopted the influence coefficient method to calculate the seal face's deformation, and determined the change law of dynamic leakage rate and gas film thickness during the start–stop stage of the mechanical seal. Considering the real gas effect, thermal effect, inertial effect, and blocking flow effect, Thomas et al. [4] determined that force deformation is the main reason for the convergent clearance formation, whereas thermal deformation forms a divergent clearance.

Fairuz et al. [5] explored the supercritical carbon dioxide dry gas seal using Ansys. The results show that the uneven temperature distribution on the seal face is the main reason for thermal deformation and that reducing the face area of the sealing ring's convective heat transfer effectively weakens thermal deformation. Ma et al. [6] numerically calculated the thermoelastic hydrodynamic characteristics and the pressure and temperature fields of the gas film layer by considering the elastic deformation, thermal deformation, and blocking flow effect of the T-groove gas seal face. Liu et al. [7] probed into the seal mechanism during the startup process and steady-state process of the mechanical seal in the case of an inclined seal face. They also studied the change laws of gas film pressure, temperature, and flow rate on the seal face by coupling Reynolds equation and energy equation. The results reveal that the dynamic mechanical seal is considerably affected by the rotating speed, whereas the static seal is almost unaffected. During the startup process, the maximum gas film thickness and the seal face temperature increase with the increase in the rotating speed.On the basis of the Reynolds equation and plastic contact model, Meng et al. [8] established a transient dynamic model of mixed friction state during the start–stop process of the mechanical seal. They also analyzed the influencing laws of axial runout and start–stop speed on the dynamic characteristics of the mechanical seal during the start–stop stage. Xu [9–11] analyzed the transient sealing characteristics of the mechanical seal during the start–stop process. The vibration characteristics under the impact condition and the cavitation effect of the liquid film were also investigated. The author's research group considered the contact force of the seal face equal to zero as the startup condition of the dry gas seal and analyzed the startup characteristics of the carbon dioxide dry gas seal by considering the slip flow effect and real gas effect. The real gas effect enhances the startup performance. However, it is inhibited by the slip flow effect. The reasonable selection of spiral groove structural parameters helps improve the startup ability of the dry gas seal and reduce the friction and wear of the seal face.

Researchers conducted in-depth investigations on the thermal effect and dynamic characteristics of dry gas seals in the stable operation stage. However, few studies were conducted on the heat generation characteristics during the startup process and in the early startup process under the coexistence of asperity contact and gas lubrication. In the present study, the statistically modified contact model and the average Reynolds equation are combined by considering factors such as material properties, surface morphology changes, and the gas film slip flow effects of the sealing ring to explore the heat generation characteristics of dry gas seals formed in series at multiple times. The adiabatic index, including the change laws and influencing factors among the components, the friction heat of asperities, and the shear heat and expansion heat of the gas film and total heat, are also considered.

2. Establishment of the seal face contact model

2.1. Contact parameters of a single asperity

The structure of the dry gas seal is shown in Figure 1a. The common combination of silicon carbide and graphite was selected for the dynamic and stationary rings, as shown in Figure 1b. The real contact behavior of the seal surface was the interaction between the surface asperities, as shown in Figure 1c. The contact deformation mainly occurred on the graphite ring because the hardness of silicon carbide was greater than that of graphite. The GT model [12] assumes that the junction surface

Preprints (www.preprints.org) | NOT PEER-REVIEWED | Posted: 9 November 2023 doi:10.20944/preprints202311.0650.v1

was equivalent to the contact between a rigid, smooth plane and a rough plane. The rotary ring with high hardness was a rigid plane, and the stationary ring with lower hardness was a rough plane.

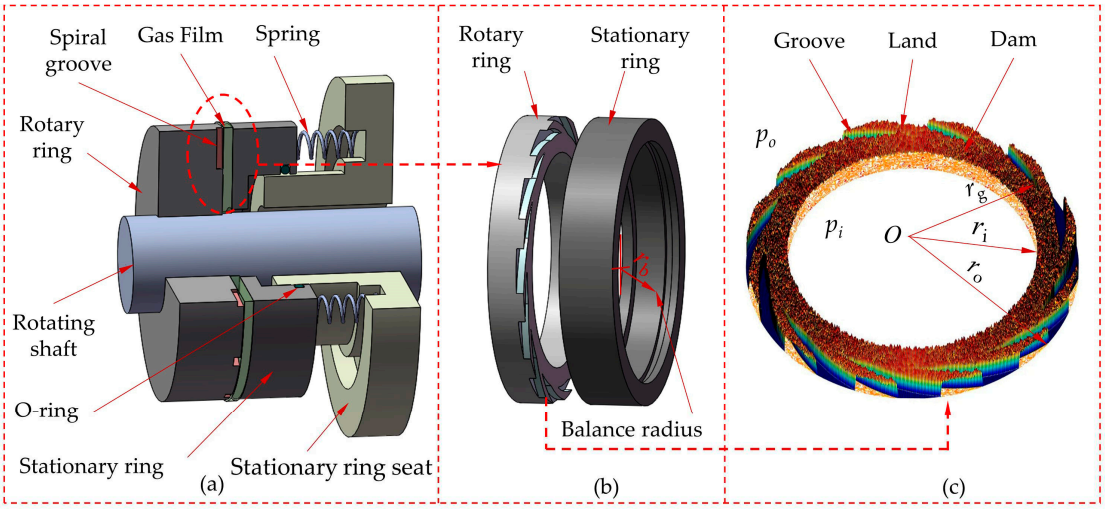

Figure 1. (**a**) The structure of DGS; (**b**) Seal rings; (**c**) The microscopic surface of seal rings.

The contact diagram of sea surfaces is exhibited in Figure 2a. As shown in Figure 2b, the asperity peak was deformed before and after a single asperity contacted the rigid plane. In Reference [13], the graphite ring was loaded, and the stress–strain characteristics were obtained, as shown in Figure 2c where z is the height of the asperities on the seal surface, d is the distance between the average asperity heights of the rough surface and the smooth rigid plane, h is the distance between the average surface heights of the rough surface and the smooth rigid plane, d_s is the height of the rough surface contour, y_s is the distance between the average asperity height of the rough surface and the average surface height line of the smooth rigid plane, R is the peak curvature radius of the asperity, and ω is the normal deformation of single asperity [16].

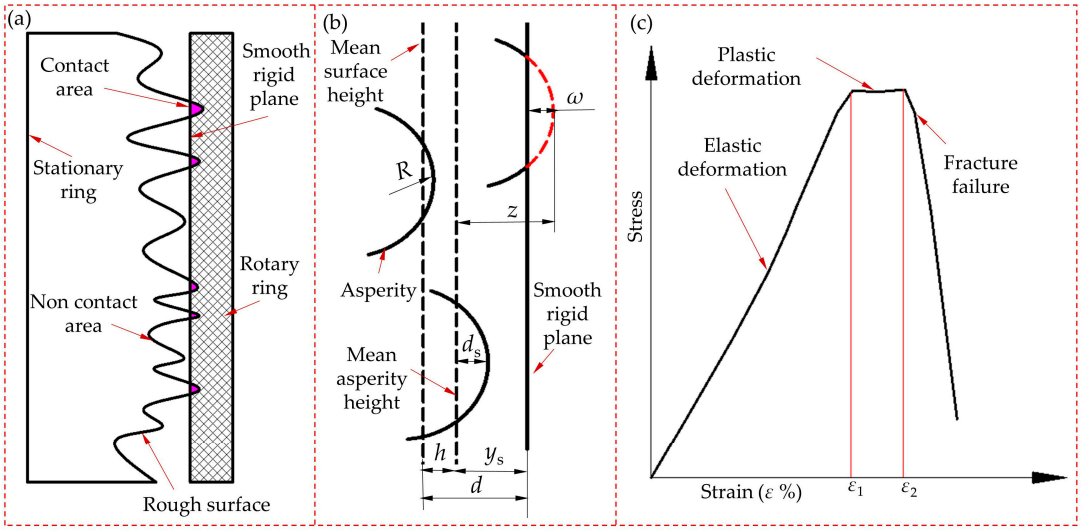

Figure 2. (**a**) End face contact of DGS; (**b**) The asperities of seal face; (**c**) Stress–strain characteristics.

$$\omega = z - d\,, \tag{1}$$

Characteristics were obtained, as shown in Figure 2c. The experimental results indicate that when $\varepsilon < \varepsilon_1$, the normal stress was linearly correlated with the strain. According to Hertzian

Preprints (www.preprints.org) | NOT PEER-REVIEWED | Posted: 9 November 2023 doi:10.20944/preprints202311.0650.v1

elasticity theory [14], the sealing ring was considered to elastically deformed in this case. When $\varepsilon_2 \le \varepsilon \le \varepsilon_1$, the stress did not change with strain or fluctuated slightly, and plastic deformation occurred according to Abbott and Firestone plastic contact theory [15]. When $\varepsilon > \varepsilon_2$, the stress decreased rapidly with the increase in strain. Moreover, the sealing ring was subjected to apparent fracture failure.

On the basis of the experimental results of Reference [13], this study assumed that the stress–strain characteristics of a single asperity on the graphite ring were the same as those of the whole graphite ring; that is,

$$\varepsilon = \frac{\Delta L}{L} = \frac{\omega}{R}, \tag{2}$$

where ΔL is normal deformation of seal ring, L is original thickness of seal ring, R is original thickness of the asperity. ω_1 *and* ω_2 are respectively the normal deformation of elastic deformation and plastic deformation:

$$\frac{\omega_1}{R} = \varepsilon_1 \ , \frac{\omega_2}{R} = \varepsilon_2 \ . \tag{3}$$

In the elastic contact stage, the average contact pressure P_t and contact area A_t of a single asperity are expressed as follows according to Hertzian elasticity theory [14]:

$$P_t = \frac{4E}{3\pi}(\frac{\omega}{R})^{\frac{1}{2}}, \tag{4}$$

$$A_t = \pi R\omega, \tag{5}$$

where E is equivalent elastic modulus. When $\omega_2 \ge \omega \ge \omega_1$, the asperity was turned from the original elastic deformation into plastic deformation, and the average contact pressure P_s of a single asperity in the plastic deformation stage is:

$$P_s = \frac{4E}{3\pi}(\frac{\omega_1}{R})^{\frac{1}{2}}, \tag{6}$$

According to Abbott and Firestone [15] plastic contact theory, the contact area A_s is expressed as follows:

$$A_s = 2\pi R\omega, \tag{7}$$

When $\omega > \omega_2$, the whole asperity lost continuous deformation and experienced fracture failure along with the rapid decline of the normal stress, all of which were the characteristics of brittle materials different from metallic materials.

2.2. Actual contact interface parameters of the dry gas seal

If the asperities on the seal surface meet the Gaussian distribution, then the probability density of the asperity height distribution is expressed as follows [16]:

$$\varphi(z) = \frac{1}{\sqrt{2\pi}\sigma_s}\exp(-\frac{z^2}{2\sigma_s{}^2}), \tag{8}$$

The number of contact asperities on the contact interface of the sealing ring is

$$\begin{aligned} N &= N_z\int_d^\infty \varphi(z)dz = N_1 + N_2 + N_3 \\ &= A_n\eta\int_d^{d+\omega_1}\varphi(z)dz + A_n\eta\int_{d+\omega_1}^{d+\omega_2}\varphi(z)dz + A_n\eta\int_{d+\omega_2}^{\infty}\varphi(z)dz \end{aligned}, \tag{9}$$

Preprints (www.preprints.org) | NOT PEER-REVIEWED | Posted: 9 November 2023 doi:10.20944/preprints202311.0650.v1

where η is the area density of asperity per unit area, and N_1, N_2, N_3, N_z are the number of asperities that undergo elastic deformation, plastic deformation, fracture failure, and all asperities on the seal face, respectively.

According to the actual situation of the dry gas seal, the maximum contact force should be less than or equal to the closing force [17]. According to the calculation, the number of asperities experiencing fracture failure was less than 0.21% of the total number of asperities. Given the small number of asperities with fracture failure and complex mechanical properties, the treatment method of the microcontact characteristics of metallic materials was taken for reference [15]. During calculation, the asperities of the fracture part were assumed to experience plastic deformation; that is,

$$N = N_z\int_d^{\infty}\varphi(z)dz = N_1 + N_2 = A_n\eta\int_d^{d+\omega_1}\varphi(z)dz + A_n\eta\int_{d+\omega_1}^{\infty}\varphi(z)dz, \quad (10)$$

where A_n is the nominal contact area, then the actual contact area of the seal contact interface is

$$\begin{aligned} A_m &= A_{tr} + A_{sr} \\ &= N\int_d^{d+\omega_1}\pi R\omega\varphi(z)dz + N\int_{d+\omega_1}^{\infty}2\pi R\omega\varphi(z)dz \end{aligned}, \quad (11)$$

where A_{tr} and A_{sr} are actual contact area of asperities elastic deformation and plastic deformation, then contact force of seal face is

$$\begin{aligned} F_m &= N_1P_tA_t + N_2P_sA_s = F_{tr} + F_{sr} \\ &= A_n\eta\int_d^{d+\omega_1}\frac{4}{3}ER^{\frac{1}{2}}\omega^{\frac{3}{2}}\varphi(z)dz + A_n\eta\int_{d+\omega_1}^{\infty}\frac{8}{3}ER^{\frac{1}{2}}\omega_1^{\frac{1}{2}}\omega\varphi(z)dz \end{aligned}, \quad (12)$$

where F_{tr} and F_{sr} are actual contact force of asperities elastic deformation and plastic deformationis.

3. Gas film pressure distribution model of the seal face

The actual gas film thickness of the seal face comprises the average gas film thickness h_0 in the dam area and the random gas film thickness caused by the roughness of the sealing surface. In particular, the heights of the asperities on the rough surface of the seal end face follow a normal distribution, and the root mean square deviation (RMSD) of the profile is σ = 1.25Ra. The comprehensive RMSD of the seal end face is $\sigma = (\sigma_{12}+\sigma_{22})^{1/2}$. σ is the comprehensive RMSD of the rough surface. Ra_1 and Ra_2 are the arithmetic mean deviations of the surface profile of the rough surface. σ_1 and σ_2 are the standard deviations corresponding to the rough surface. The average Reynolds equation derived by Makino et al. [18] under isothermal and compressible fluid conditions is as follows:

$$\frac{\partial}{\partial r}\left(\psi_q\psi_r\frac{rh^3}{\eta}\frac{\partial p^2}{\partial r}\right) + \frac{1}{r}\frac{\partial}{\partial\theta}\left(\psi_q\psi_\theta\frac{h^3}{\eta}\frac{\partial p^2}{\partial\theta}\right) = 12\omega r\frac{\partial}{\partial\theta}(ph) + 12\omega r\frac{\partial}{\partial\theta}(\psi_s\sigma p), \quad (13)$$

where ψ_q is slip flow factor, which based on the F-K slid flow model [19]. ψ_θ and ψ_r are the circumferential and radial pressure flow factors, respectively. ψ_s is shear flow factor.

$$\begin{cases} Q_c = D/6 \\ \begin{cases} Q_p = D/6 + 1.0162 + 1.0653/D - 2.1354/D^2 \quad (D > 5) \\ Q_p = 0.13852D + 1.25087 + 0.15653/D - 0.00969/D^2 \quad (0.15 < D < 5) \\ Q_p = -2.22919D + 2.10673 + 0.01653/D - 0.0000694/D^2 \quad (0.01 < D < 0.15) \end{cases} \\ \psi_q = Q_p/Q_c = 1 + 6aK_n \end{cases}, \quad (14)$$

Preprints (www.preprints.org) | NOT PEER-REVIEWED | Posted: 9 November 2023 doi:10.20944/preprints202311.0650.v1

where D is the characteristic inverse Knudsen number. The expressions given are presented as follows:

$$\psi_r = 1 + g \cdot (\sigma / h)^2 \cdot \left(1 - \frac{e^2}{g} \frac{\gamma}{\gamma + 1}\right), \tag{15}$$

$$\psi_\theta = 1 + g \cdot (\sigma / h)^2 \cdot \left(1 - \frac{e^2}{g} \frac{1}{\gamma + 1}\right), \tag{16}$$

$$\psi_s = (\sigma_1 / \sigma)^2 \cdot \psi_{s1} - (\sigma_2 / \sigma)^2 \cdot \psi_{s2}, \tag{17}$$

$$\psi_{si} = e \cdot (\sigma_i / h)^2 \cdot \frac{1}{\gamma_i + 1}, \tag{18}$$

$$e = 3 - (6aK_n) / (1 + 6aK_n), \tag{19}$$

$$g = 3 - (12aK_n) / (1 + 6aK_n), \tag{20}$$

where a is the surface adaptation coefficient, which is the reflection type after the collision between gas molecules and the boundary wall, generally taken as 1, and γ is the morphology of rough surface in both vertical and horizontal directions, 0 is represents transverse, infinity represents longitudinal, and 1 is represents isotropic.

4. Heat generation model on the seal face during the startup process

The two sealing rings of the dry gas seal were in contact during the early startup process, and the main heat sources on the seal face at different times were the friction heat of asperities, the viscous shear heat of the gas film, and the expansion heat (heat absorbed by the gas film under adiabatic conditions). The increase in the rotating speed disengaged the sealing rings from each other, thereby forming a stable gas film. In this case, the seal face heat was mainly derived from the viscous shear heat and the expansion heat of the gas film.

4.1. Friction heat model of asperities

The dynamic and static sealing rings were in contact in the early startup process. They also maintained a certain contact pressure. In this case, the relative movement between the two rings led to the contact friction heat of the asperities. The following expression of the friction heat on the rough surface of the dry gas seal was derived from the relevant literature [20]:

$$W_m = M_m \cdot \omega = \frac{P \cdot \left[\pi(r_o^2 - r_i^2) - \frac{\pi}{2}(r_o^2 - r_g^2)\right]}{\pi \cdot (r_o - 2r_i + r_g)} \cdot \left[\pi \cdot f \cdot (\frac{r_o^2}{2} - r_i^2 + \frac{r_g^2}{2})\right] \cdot \frac{\pi \cdot n}{30}, \tag{21}$$

where f is the solid friction coefficient of the seal face, which is obtained through experimental measurement, M_m is friction torque, n is rotating speed.

4.2. Gas film shear heat model

When the spiral groove-type dry gas seal started running, a gas film with an equivalent thickness of h was found between seal faces. Certain heat was generated during the sealing operation because of the friction in the gas. The friction heat in the groove platform area was calculated based on Newton's viscous shear law, which was the sum of the heat generated in the sealing groove platform area and the heat generated in the seal dam area [21].

Preprints (www.preprints.org) | NOT PEER-REVIEWED | Posted: 9 November 2023 doi:10.20944/preprints202311.0650.v1

$$W_J = \int_{r_i}^{r_g} \frac{2\pi\mu\omega^2}{h_0} r^3 dr + \int_{r_g}^{r_o} \frac{2\pi\mu\omega^2}{h_0 + h_g} r^3 dr \,, \tag{22}$$

4.3. Gas film expansion heat model

The sealing gas pressure was generally higher than the ambient pressure. Thus, the dynamic pressure effect prompted the gas pressure to increase when the gas was flowing from the outer diameter to the inner diameter of the sealing ring. Then, the gas pressure decreased rapidly at the outlet, resulting in gas depressurization and expansion. The gas needed to absorb heat because of expansion. If enough heat could not be rapidly obtained from the environment, heat could only be acquired inside the seal end face. Thus, the gas temperature declined. Polycarpou and Etsion [22] solved the flow quantity of the rough surface of the seal face. The mass leakage rate of the seal face can be acquired as follows:

$$\begin{aligned} Q = \int_0^{2\pi} qrd\theta &= -\frac{1}{R_g T_o} \frac{\psi_r h_0^{\,3} r}{12\mu} \frac{\partial}{\partial r} \int_0^{2\pi} \left(\frac{p^2}{2} + \frac{6\lambda_a p_a p}{h_0} \right) d\theta \\ &= -\frac{\pi\psi_r h_0^{\,3} r}{12\mu R_g T_o} \frac{\partial}{\partial r} \left(p^2 + 12 K_n p_a p \right) \end{aligned} \,, \tag{23}$$

where ψ_r is the average pressure flow coefficient, μ is the gas dynamic viscosity, R_g is the gas constant, p_a is the pressure at the inner diameter of the seal ring, i.e. the ambient pressure, λ_a is the average free path of the gas at p_a, K_n is the Knudsen number, which describes the collision of molecules during fluid motion.

The expansion heat of gas absorbing heat between two points [23]:

$$W_p = \sum_{i=1}^{M} Q c_p \left(T_i - T_{i-1} \right) = \sum_{i=1}^{M} Q \frac{R_g}{k-1} \left(T_i - T_{i-1} \right) , \tag{24}$$

where T_i(i=1,2,…,M) is the temperature at the radial point i, and k is the gas adiabatic index, c_p is the gas specific heat capacity.

According to the thermodynamic process equation, the following exists when the gas on the seal face is an ideal gas:

$$\frac{T_i}{T_{i-1}} = \left(\frac{p_i}{p_{i-1}} \right)^{\frac{k-1}{k}} , \tag{25}$$

where p_i(i=1,2,…,M) is the pressure at the radial point i. From formulas (24) and (25), it can be concluded that

$$W_p = \sum_{i=1}^{N} Q \frac{R_g T_o}{k-1} \left(1 - \left(\frac{p_i}{p_{i-1}} \right)^{\frac{k-1}{k}} \right) , \tag{26}$$

5. Calculation parameters by the experimental

The sealing ring's surface morphology and friction coefficient are important initial conditions for the thermal analysis of dry gas seals during the startup process. Accurate surface morphology and friction coefficient of the sealing ring play an important guiding role in judging the friction heat of asperities and the gas film thickness during startup and analyzing critical disengagement conditions. In traditional studies, these two parameters are considered initial constant values from the literature. However, the surface morphology and friction coefficient vary in the actual operation

Preprints (www.preprints.org) | NOT PEER-REVIEWED | Posted: 9 November 2023 doi:10.20944/preprints202311.0650.v1

process. In particular, the friction coefficient is a function of velocity and contact pressure. In this study, these two parameters were experimentally determined.

5.1. Surface morphology experiment and results

According to the theory proposed by McCool [24], the surface morphology detection principle for the rotary and stationary rings of the dry gas seal is as follows. The profile spectrum function of the rough surface was characterized by measuring the RMSD R_q and root mean square slope difference (RMSSD) R_{dq} of the rough surface profile. Then, the spectral moment of the profile spectrum function was solved through the surface's profile spectrum function to solve the statistical parameters under the real morphology of the sealing ring. Figure 3a is the test diagram of the surface morphology parameters of the sealing ring measured by the roughness profilometer testing integrated machine (SEF680). The measuring range of this machine is 0 mm to 50 mm for Z and 0 mm to 100 mm for X, the stylus radius is 2 μm, and the sampling length j_r is 0.25 mm. In the experiment, the stationary ring was made of carbon graphite, and the rotary ring was made of silicon carbide. In addition, the measurement speed and evuation length were set to 0.2 mm/s and $j_n = 5j_r = 1.25$ mm, respectively. The stationary ring has 10 positions, randomly chosen on the seal faces of the stationary and rotary rings. The average value was taken by conducting measurements at each position twice. The typical profile curves of the surface roughness of the stationary and rotary rings are displayed in Figure 3b. The measured RMSD and RMSSD of the surface profile at 10 different positions on the surfaces of the rotary and stationary rings were $R_{qs} = 0.0590$, $R_{dqs} = 0.0608$, $R_{qr} = 0.0670$, and $R_{dqr} = 0.056$. The statistical parameters of the surface morphology were calculated as follows: $\alpha = 5.646$, $y_s = 0.085$ μm, $\sigma_s = 0.082$ μm, $R = 3.655$ μm^2, $\eta = 0.148$ μm^{-2}.

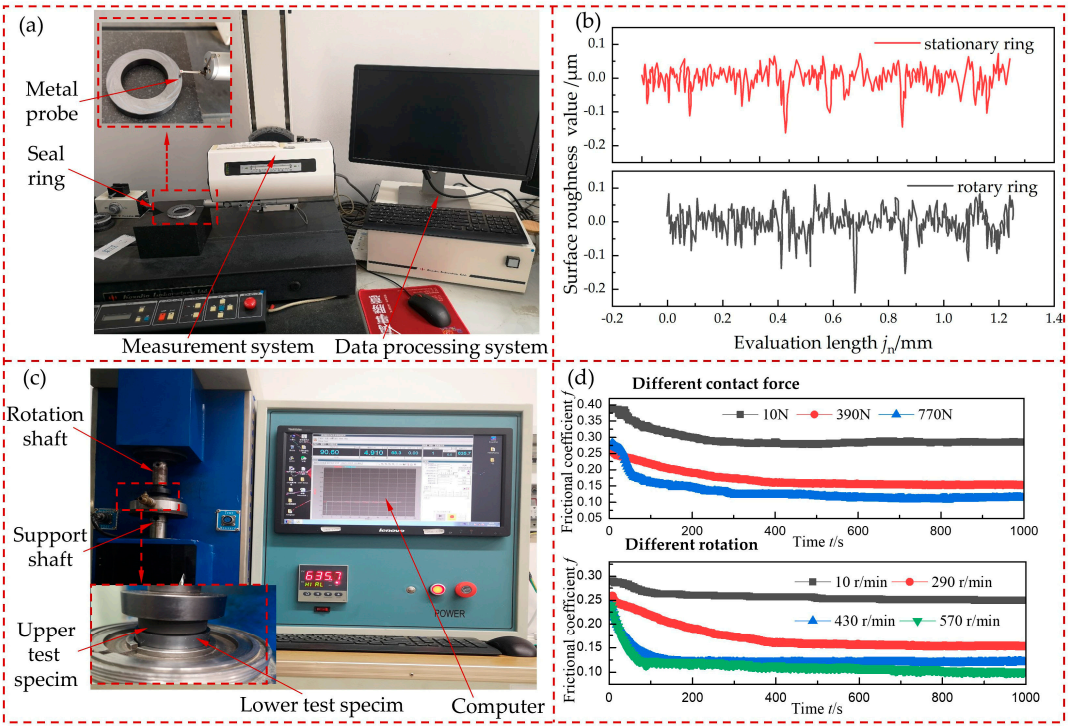

Figure 3. Surface morphology and friction coefficient measurement. (**a**) Experimental device of surface profiler; (**b**) Surface contour curve of seal rings; (**c**) Friction and wear machine; (**d**) Frictional coefficient.

5.2. Friction coefficient experiment and results

The accurate characterization of the friction coefficient during the startup process directly affects the friction and thermal characteristics of the seal face. The friction coefficient of the silicon carbide

Preprints (www.preprints.org) | NOT PEER-REVIEWED | Posted: 9 November 2023 doi:10.20944/preprints202311.0650.v1

sealing ring and graphite sealing ring was measured by the friction and wear testing machine, as shown in Figure 3c. The variation laws of the friction coefficient with rotating speed and contact pressure are shown in Figure 3d. These variation laws laid the foundation for the calculation of friction heat during the startup process. The central composite experimental design was used to conduct a response surface analysis experiment on the friction coefficient with two factors and five levels [25] by taking the friction coefficient (Y) of the sealing surface as the response value and the rotating speed (n, m/s) and contact pressure (p_c, MPa) as the independent variables (five levels were taken for each factor, coded by −2, −1, 0, 1, and 2). A total of 15 experimental groups were completed, of which 12 groups were factorial experiments, and 3 groups were zero. In each group, the experiment was repeated twice, and the average value was taken. Finally, the experimental data were subjected to quadratic polynomial regression fitting via the statistical software of MINITAB to acquire the ternary quadratic regression equations of the friction coefficient with the rotating speed and contact pressure, as follows:

$$f = 0.41946 - 2.6195^{-4} n - 1.54543^{-6} p_c + 1.71349^{-7} n^2 + 2.54309^{-12} {p_c}^2 + 6.54081^{-11} n p_c \quad (27)$$

6. Model verification

The material characteristic parameters and geometric dimension parameters of the dry gas seal ring are listed in Table 1 [26–28]. The startup process of the dry gas seal involves many theories, such as solid friction and gas lubrication. Thus, the asperity contact model and the gas film opening force of the dry gas seal were used for respective verification.

Table 1. Structure parameters and material parameters of the model.

Parameter	value	Parameter	value
Hardness of soft materials H/GPa	0.7	Outer diameter of sealing ring r_o/mm	77.78
Equivalent elastic modulus E/GPa	23.65	Helix angle α/(°)	15
Maximum contact pressure factor K	0.577	Ratio of groove to dam γ	1
plasticity index ψ	18.6	number of groove N_g	12
Groove root radius of Seal ring r_g/mm	69	Rotary ring	SiC
Inner diameter of seal ring r_i/mm	58.42	Stationary ring	C

Note: 1. Equivalent elastic modulus: The comprehensive effect of the elastic modulus of two elastic materials. 2. Maximum contact pressure factor: The hardness coefficient of softer materials.

The contact force calculation result obtained through the current model was compared with the result of the classical contact models [18,29–31]. The variation trends of each model are displayed in Figure 4a. The results obtained in this study were consistent with the trend of each classical model and were highly approximate with the results of the GW model, which verified the conclusion of McCool [32], i.e., the GW model can accurately judge the contact characteristics of brittle materials. The working condition parameters from Xu [2], which were chosen to verify the numerical calculation result of the average Reynolds equation, are shown in Figure 4b. The inlet pressure was 3.03 MPa, the maximum deviation of the obtained result was 2.77%, and the average deviation was 2.5%. The finite element numerical method was adopted in the literature, and the finite element difference method was used in this study. Thus, deviations resulted from the different numerical calculation methods.

Preprints (www.preprints.org) | NOT PEER-REVIEWED | Posted: 9 November 2023 doi:10.20944/preprints202311.0650.v1

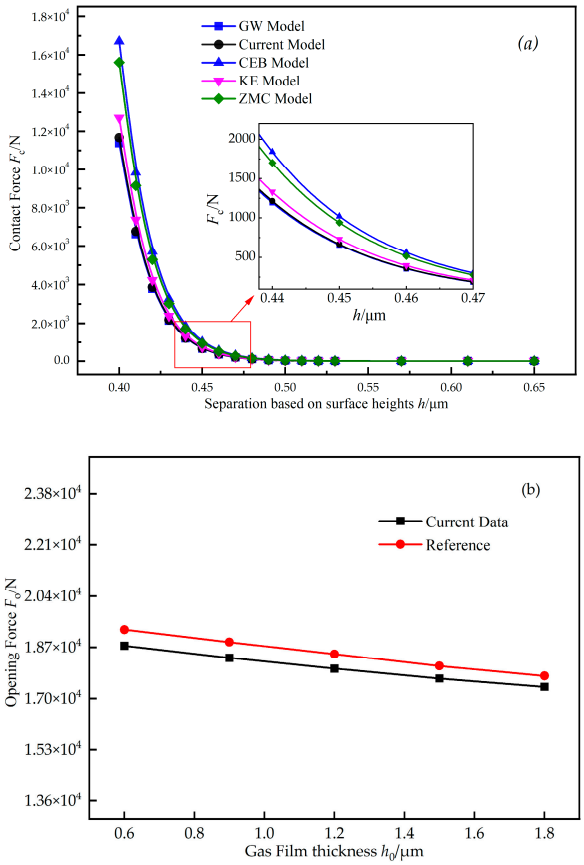

Figure 4. (**a**) Contact force of different contact models; (**b**) Verification of the average Reynolds equation.

7. Result analysis

7.1. Influence of gas slip flow effect on startup thermal effect

As shown in Figure 5a, three typical startup modes of the dry gas seal were chosen: constant acceleration, exponential acceleration, and Harrision acceleration. The heat generation characteristics of the dry gas seal under three different startup modes in the startup process formed by multiple time series connections (0–5 s) were analyzed. Figure 5 shows that the gas slip flow effect led to an increasing trend of total gas heat. This increasing trend occurred because when the slip flow was used as the basic calculation model, the slip flow effect was equivalent to the decrease in gas viscosity, the viscous shearing effect was weakened, and the hydrodynamic pressure effect was reduced. These phenomena decreased the gas film pressure. Under the constant closing force, the contact pressure of the seal face asperities was high, increasing the solid friction heat on the seal face. The heat absorbed by gas expansion was directly proportional to the leakage rate. Given the slip flow effect, the decrease in gas viscosity increased the leakage rate, resulting in an increase in the heat absorbed by gas expansion. Overall, the three startup modes showed considerable heat in the early startup process and stable heat in the later startup process. In the form of exponential acceleration, 10^4-magnitude heat could be reached within 1 s of startup. This scenario was extremely unfavorable to the dry gas seal, with a risk of instability. A large amount of friction heat led to the extremely uneven heating of the sealing ring, which was prone to hot cracking. The heat increase in the Harrision acceleration mode was gentle. Moreover, the period was long, which was conducive to the heat dissipation of the sealing system. The heat generation perspective indicates that the Harrision acceleration mode is the most beneficial for sealing stability.

 doi:10.20944/preprints202311.0650.v1

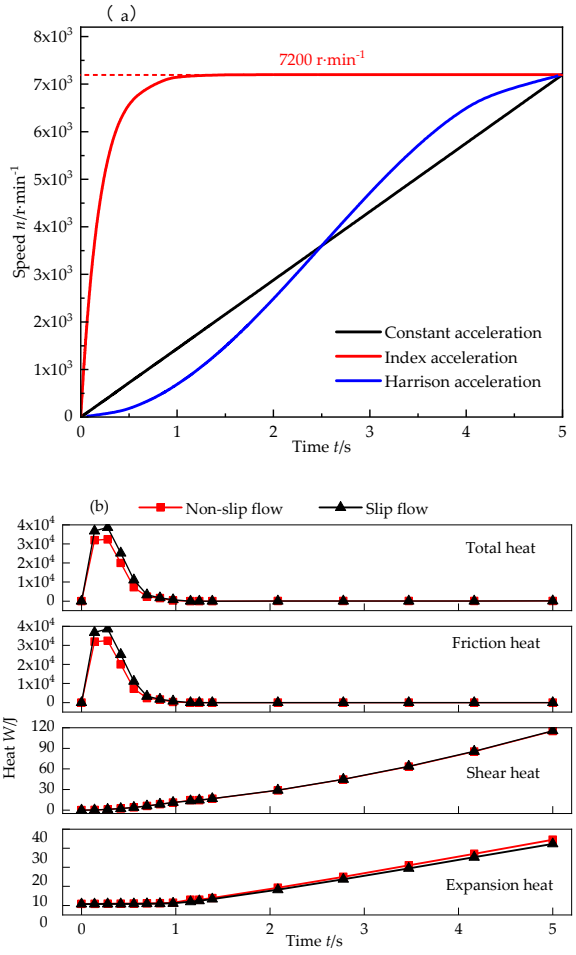

Preprints (www.preprints.org) | NOT PEER-REVIEWED | Posted: 9 November 2023 doi:10.20944/preprints202311.0650.v1

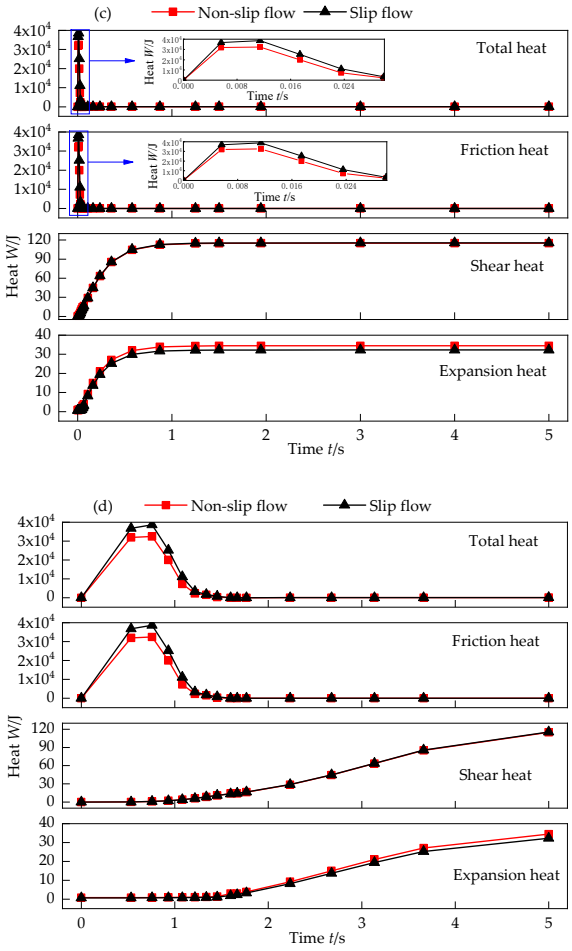

Figure 5. Heat of different acceleration modes considering slip flow effects. (**a**) Three acceleration methods; (**b**) Constant acceleration; (**c**) Index acceleration; (**d**) Harrision acceleration.

7.2. Influence of sealing ring surface morphology on startup thermal effect

The influence of the microsurface morphology of the sealing ring on the heat generation characteristics during the startup process is shown in Figures 6 and 7. The surface morphology parameters of the asperities of the sealing ring exerted certain influences on the startup process of the dry gas seal. In the early startup process, the morphology parameters mainly affected the friction heat generation on the seal face. In the later startup process, the morphology parameters influenced the shear heat and expansion heat of the gas film on the seal face by affecting the film thickness. The peak curvature radius of asperities is an important parameter of microsurface morphology. Figure 6 shows the influencing laws of the peak curvature radius of asperities on the heat generation characteristics of the dry gas seal during the startup process. During the whole startup process, the heat of the seal face changed obviously with the increase in the rotating speed. However, the influence of the peak curvature radius of asperities on heat characteristics during the startup process was relatively weak. Changing the peak curvature radius of asperities would increase the seal face contact force, thereby increasing the friction heat during the startup process. When the rotating speed was 1000 r/min, the curvature radius of asperities increased from 1 μm to 5 μm, and the friction heat increased from 36635 J to 36800 J, with an increase of 0.45%. Moreover, the growth fluctuation was small. The reason is that an adaptive adjustment process occurred during the startup process, and the contact force could be adjusted by adjusting the film thickness. The shear heat and expansion heat of the gas film were not obvious in the early startup process. Thus, the total heat was mainly the friction heat of asperities. The analysis indicated that the influence trend of the area density of asperities on the seal face heat

Preprints (www.preprints.org) | NOT PEER-REVIEWED | Posted: 9 November 2023 doi:10.20944/preprints202311.0650.v1

during the startup process was the same as the peak curvature radius of asperities. Therefore, it is not detailed in the present study.

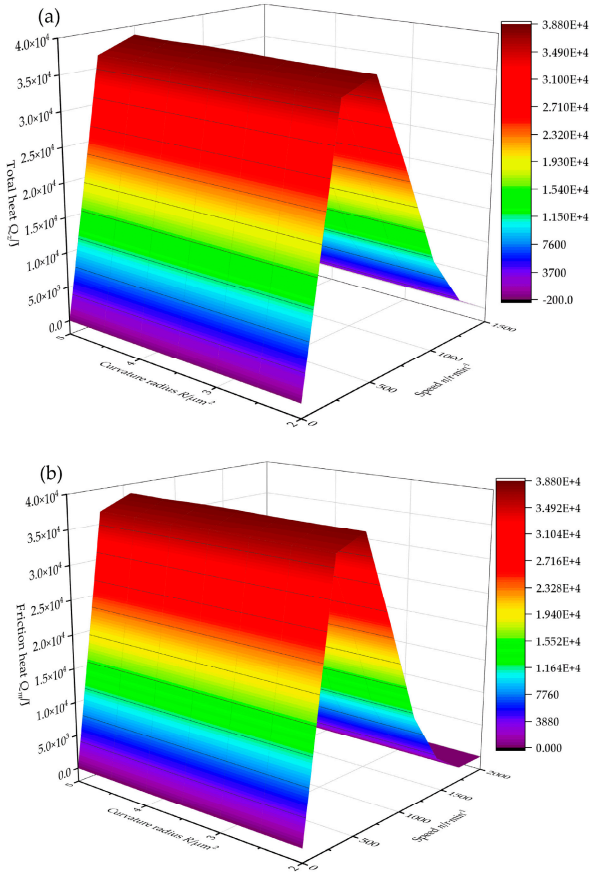

Preprints (www.preprints.org) | NOT PEER-REVIEWED | Posted: 9 November 2023 doi:10.20944/preprints202311.0650.v1

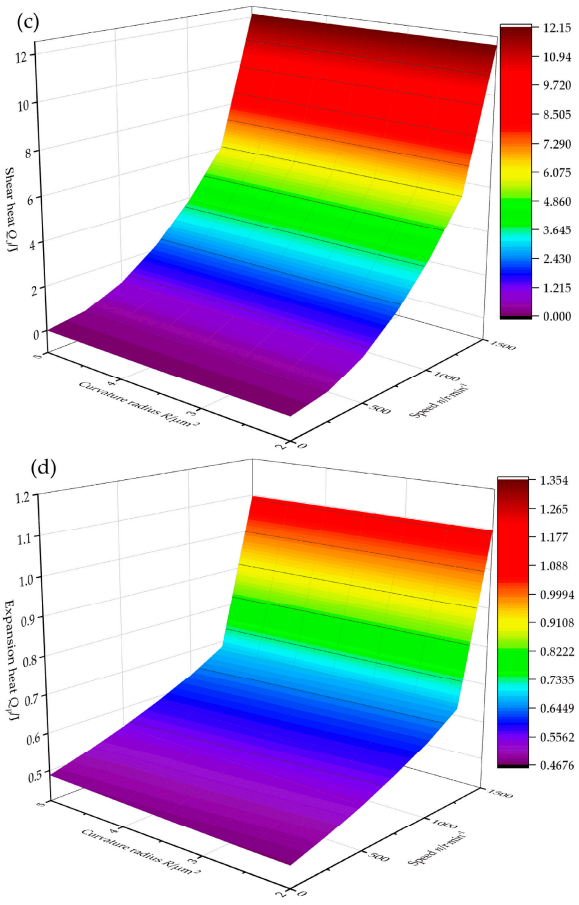

Figure 6. The The influence of curvature radius on heat. (**a**) Total heat; (**b**) Friction heat; (**c**) Shear heat; (**d**) Expansion heat.

Figure 7 shows the height distribution of asperities on the seal surface during the startup process of the dry gas seal and the influence of the standard deviation on thermal characteristics. Figure 8 shows that the total heat and friction heat of the seal face first increased and then decreased with the increase in the rotating speed. Then, they increased with the increase in the standard deviation of the height distribution of asperities on the surface. The standard deviation of the height distribution of asperities could reflect the roughness of the seal face: the greater the standard deviation of the asperity height distribution is, the greater the roughness, the fluctuation of the seal face's roughness peak, and the friction resistance are. This scenario led to an increase in heat.

 doi:10.20944/preprints202311.0650.v1

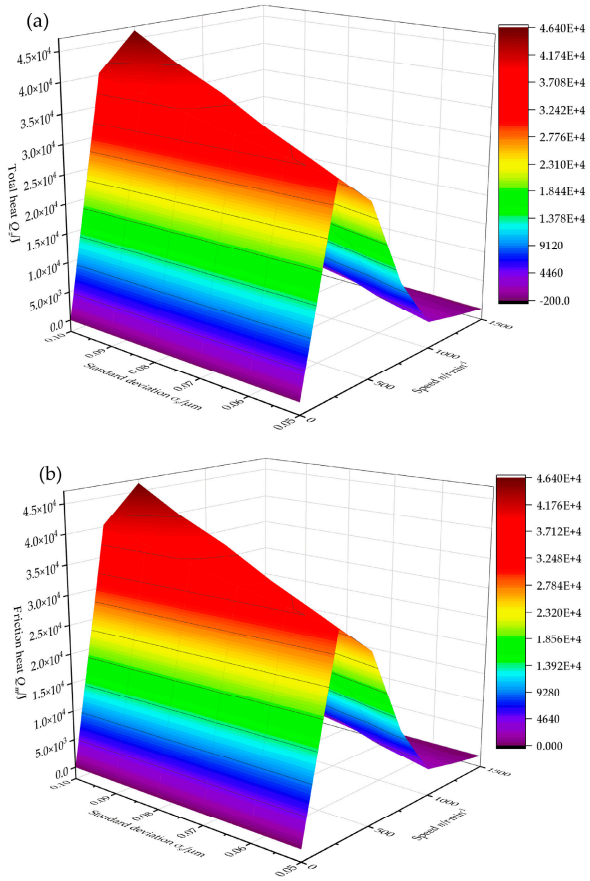

Preprints (www.preprints.org) | NOT PEER-REVIEWED | Posted: 9 November 2023 doi:10.20944/preprints202311.0650.v1

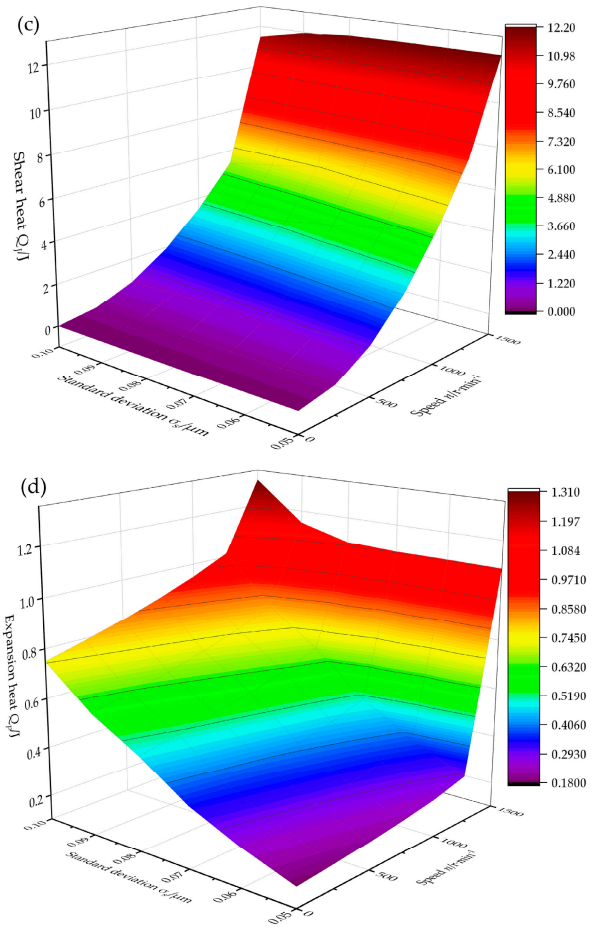

Figure 7. The influence of standard deviation on heat.. (**a**) Total heat; (**b**) Friction heat; (**c**) Shear heat; (**d**) Expansion heat.

The shear heat of the gas film increased with the increase in the rotating speed and decreased with the increase in the standard deviation of the surface asperities' height distribution, because the increase in roughness increased the peak–valley difference and the equivalent film thickness but weakened the intermolecular interaction, resulting in the decrease in shear heat. The expansion heat of the gas film on the end face increased with the increase in the rotating speed and the standard deviation of the surface asperities' height distribution because the increase in the equivalent gas film thickness prompted the increase in the leakage. The work of gas expansion was directly proportional to the leakage rate, thereby increasing the gas expansion heat.

7.3. Influence of working pressure on startup thermal effect

The changes in the heat characteristics on the seal face during the startup process are exhibited in Figure 8. During the whole startup process, the seal face heat initially increased sharply, then declined rapidly, and finally increased slowly. The heat in the early stage rapidly increased because the seal face was not disengaged in the early startup process, and friction occurred between the asperities on the seal face, resulting in considerable friction heat. However, the dynamic pressure effect of the seal face was enhanced, and the film thickness gradually increased with the increase in the rotating speed. Moreover, the seal face was disengaged, and the friction heat no longer existed. The increase in heat during the later startup process entirely resulted from the interaction between shear heat and expansion heat of the gas film. The friction heat generated by the seal face asperities in the early startup process was particularly obvious with the increase in the working pressure. The friction heat of the asperities reached 1.6×10^6 J when the working pressure reached 10 MPa. With the

Preprints (www.preprints.org) | NOT PEER-REVIEWED | Posted: 9 November 2023 doi:10.20944/preprints202311.0650.v1

increased working pressure, the friction heat of the seal face asperities lasts long. This scenario had a negative impact on the stable operation of the dry gas seal and even led to the hot cracking of the sealing ring, leading to seal failure. The shear heat and expansion heat of the gas film were much smaller than the friction heat of asperities. However, no linear relations were found. The shear heat and expansion heat of the gas film presented an increasing trend because the rotating speed was accelerated in the startup process. However, the shear heat of the gas film was an exothermic process, whereas the expansion heat was an endothermic process, reaching an offset effect. Overall, the seal face heat during the startup process was always under a net growth state and increased with the acceleration of the rotating speed.

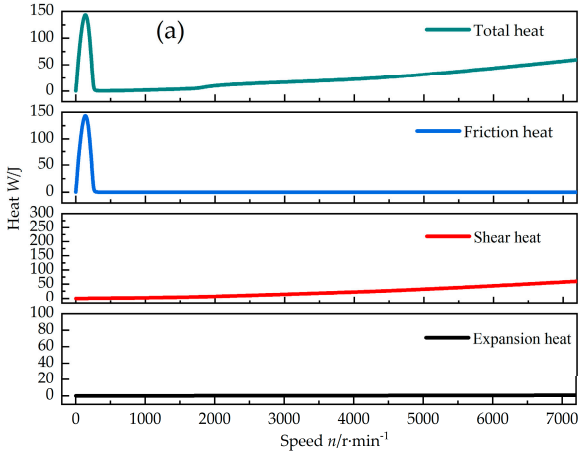

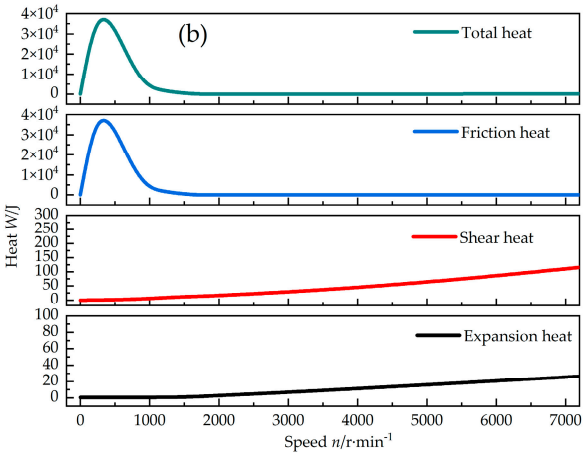

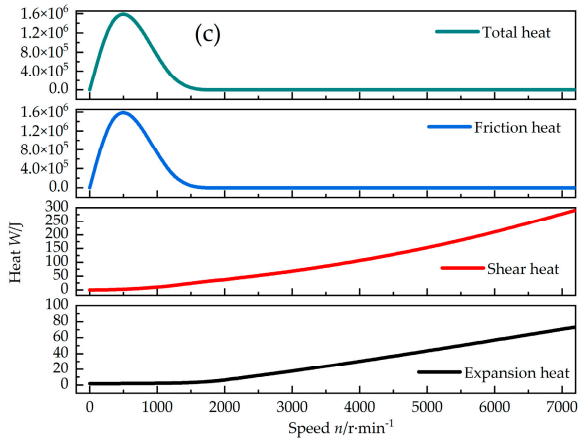

Figure 8. Thermal characteristics under different working pressures. (**a**) Operating pressure P_o = 0.303 MPa; (**b**) Operating pressure P_o = 4.5852 MPa; (**c**) Operating pressure P_o = 10 MPa.

8. Conclusions

The stable operation of dry gas seals is affected by the complicated heat generation characteristics in the startup process. In this study, the statistically modified contact model and the average Reynolds equation were combined by considering the adiabatic index of the dry gas seal system to explore the heat generation characteristics. The change laws and influencing factors, such as the friction heat of asperities and the shear heat and expansion heat of the gas film and total heat, were also analyzed. Finally, the following conclusions were drawn:

1. The friction heat of the dry gas seal is much greater than the expansion heat and shear heat of gas during the startup process. However, the time course of friction heat is short and mainly concentrated in the early startup process. It disappears rapidly with the increase in the rotating speed. However, the shear heat and expansion heat of the gas film on the seal face last long;
2. The heat generated by the shear heat of the gas film is greater than the heat absorbed by the expansion heat in the later startup process. The heat of the whole seal face continues to increase with the increase in the rotating speed. In this case, the heat mainly comes from the shear heat of the gas film. The slip flow effect of gas film leads to an increase in heat during the startup process;
3. Despite constant acceleration, exponential acceleration, or Harrision acceleration modes, the heat changes are uneven during the startup process. In particular, the heat changes violently in the early stage and slowly in the later stage. The Harrision acceleration mode is the most conducive to sealing stability;
4. The startup process involves various transient characteristics (including mechanical characteristics and heat generation characteristics of the seal face, thermal deformation characteristics of the sealing ring, and heat transfer characteristics of the sealing ring and sealing cavity). The follow-up research will focus on coupling various factors to study comprehensively the nonsteady performance of dry gas seals during the startup process.

Author Contributions: Conceptualization, H.X. and X.S.; methodology, Q.D.; software, Q.D. and W.M; validation, Q.D., X.S. and H.X.; formal analysis, Q.D.; investigation, H.X. and X.S.; data curation, Q.D.; and X.S.; writing—original draft preparation, Q.D.; writing—review and editing, Q.D and X.S.; visualization, W.M.; supervision, W.M.; project administration, H.X; funding acquisition, H.X. All authors have read and agreed to the published version of the manuscript.

Funding: This research was funded by Special Youth Fundamental Research of Yunnan Province (Grant No. 202101AU070019), Talent Training Project of Kunming University of Technology (Grant No.KKZ3202005059).

Data Availability Statement: The datasets used or analyzed during the current study are available from the corresponding author upon reasonable request.

Acknowledgments: In this section, you can acknowledge any support given which is not covered by the author contribution or funding sections. This may include administrative and technical support, or donations in kind (e.g., materials used for experiments).

Conflicts of Interest: The authors declare no conflict of interest.

References

1. Su, H.; Rahmani, R.; Rahnejat,H. Thermohydrodynamics of bidirectional groove dry gas seals with slip flow. *International Journal of Thermal Sciences*, **2016**, *110*, pp. 270–284.
2. Xu,J.; Peng X.; Bai, X.; et al. Effects of surface micro-scale and thermal viscosity on sealing performance of spiral–grooved dry gas seal. *CIESC Journal*, **2013**, *64*, pp. 3291–3300.
3. Salant, R.F.; Cao, B. Unsteady analysis of a mechanical seal using Duhamel's method. *Journal of Tribology*, **2005**, *127*, pp. 623–631.
4. Brunetière, N.; Thomas, S.; Tournerie, B. The parameters influencing high-pressure mechanical gas face seal behavior in static operation. *Tribology Transactions*, **2009**, *52*, pp. 643–654.
5. Fairuz, Z.M.; Jahn, I.; Rahman, R.A. . The effect of convection area on the deformation of dry gas seal operating with supercritical CO_2. *Tribology International*, **2019**, *137*, pp. 349–365.

6. Ma, C.; Bai, S.; Peng, X. Thermoelastohydrodynamic characteristics of T-grooves gas face seals. *International Journal of Heat and Mass Transfer*, **2016**, *102*, pp. 277–286.
7. Liu, Y.; Liu, W.; Li, Y.; et al. Mechanism of a wavy-tilt-dam mechanical seal under different working conditions. *Tribology International*, **2015**, *90*, pp. 43–54.
8. Meng, X.; Peng, X.; Wang, L. Axisymmetric dynamic model and seal behavior analysis of mechanical seals during startup and shutdown operation. *CIESC Journal*, **2011**, *62*, pp. 1620–1625.
9. Xu, L. Transient dynamic characteristics of upstream pumping mechanical seal. Master·s thesis, China University of Petroleum(east china), Qingdao, 2018.
10. Xu, L.; Hao, M.; Yuan, X.; et al. Dynamic analysis for vibration and impact of liquid film sealing. *Journal of vibration and shock*, **2020**, *39*, pp. 58–65.
11. Xu, L.; Wand, Y.; Zhang, F.; et al. Lubrication characteristics of spiral mechanical seals during transient start-up. *China Mechanical Engineering*, **2020**, *31*, pp 1891-1900.
12. Greenwood J.A.; Tripp J.H. The contact of two nominally flat rough surfaces. *Proceedings of the Institution of Mechanical Engineers*, **1970**, *185*, pp. 625–634.
13. Dong,M.; Gong, J.; Lyu, J.; et al. Tribology design of sealing materials using plastic index. *Surface Technology*, **2017**, *45*, pp. 180–185.
14. Johnson, K.L. *Contact mechanics*, 1st ed.; Cambridge University Press: Cambridge, England. 1985; pp. 84–106.
15. Abbott, E.; Firestone, F. Specifying surface quality: a method based on accurate measurement and comparison. *Mechanical Engineering*.**1933**,*107*, pp. 569–572.
16. Greenwood, J.A.; Williamson, J.B.P. Contact of nominally flat surfaces. *Proceedings of the Royal Society of London. Series A, Mathematics And Physical Sciences*, **1966**, *295*, pp. 300–319.
17. Fan, Y.; Song, P.; Xu, H. Study on startup operation of dry gas seal with steam lubrication[J]. *CIESC Journal*, **2020**, *71*, pp. 3671–3680.
18. Makino, T.; Morohoshi, S.; Taniguchi, S. Application of average flow model to thin film gas lubrication.*Journal of Tribology*, **1993**,*115*, pp 185–190.
19. Fukui,S.; Kaneko, R. A database interpolation of Poiseuille flow rates for high Kundsen number lubrication problems. *ASME Journal of Tribology*, **1990**,*112*, pp. 78–83.
20. Song, X. Analysis and Solution of Friction Heat in Mechanical Seals. *Science-Technology Enterprise*, **2013**, *4*, pp. 271,273.
21. Chan, W.; Song, P. Research on heat equilibrium film thickness of spiral groove dry gas seal.lubrication engineering, **2015**, *40*, pp. 5–8.
22. Polycarpou, A.A.; Etsion, I. Static sealing performance of gas mechanical seals including surface roughness and rarefaction effects.*ASME Journal of Tribology*, **1998**, *41*, pp. 531–536.
23. Zhu,M.; Liu, Y.; Lin, Z.; et al. *Engineering Thermodynamics*, 2nd ed.; Tsinghua University Press: Beijing, China. 2011; pp. 22–23.
24. McCool, J.I. Relating profile instrument measurements to the functional performance of rough surfaces. *Journal of Tribology*, **1987**, *109*, pp. 264–270.
25. Peng, L.; Gao, X.; Chen, K. Catalytic upgrading of renewable furfuryl alcohol to alkyl levulinates using $AlCl_3$ as a facile, efficient, and reusable catalyst. *Fuel*, **2015**, *160*, pp. 123–131.
26. Gabriel, R.P. Fundamentals of spiral groove noncontacting face seals. *Lubrication Engineering*,**1994**, *50*, pp. 215–224.
27. Hu, Q.; Sun, J.; Ma, C.B.; et al. Theoretical prediction of mixed frictional heat of mechanical seals based on shoulder-shoulder contact model of asperities. *Journal of Mechanical Engineering*, **2017**, *53*, pp. 102–108.
28. Itzhak, G. A Transient Dynamic Analysis of Mechanical Seals Including Asperity Contact and Face Deformation. *Tribology Transactions*, **2002**, *45*, pp. 284–293.
29. Chang, W.R.; Etsion, I.; Bogy, D.B. An elastic–plastic model for the contact of rough surfaces. *Transactions of the ASME Journal of Tribology*, **1987**, *109*, pp. 257–263.
30. Kogut, L.; Etsion, I. Elastic-plastic contact analysis of a sphere and a rigid flat. *Joural of applied mechanics*, **2002**, *69*, pp. 657–662.
31. Zhao, Y.; Maietta, D.M.; Chang, L. An asperity microcontact model incorporating the transition from elastic deformation to fully plastic flow. *Journal of Tribology*, **2000**, *122*, pp. 86–93.
32. McCool, J.I. Comparison of models for the contact of rough surfaces. *Wear*, **1986**, *107*, pp. 37–60.